Supporting Information for

ORIGINAL ARTICLE

Nanoparticles with rough surface improve the therapeutic effect of photothermal immunotherapy against melanoma

Jiao Xue, Yining Zhu, Shuting Bai, Chunting He, Guangsheng Du, Yuandong Zhang, Yao Zhong, Wenfei Chen, Hairui Wang, Xun Sun*

Key Laboratory of Drug-Targeting and Drug Delivery System of the Education Ministry and Sichuan Province, Sichuan Engineering Laboratory for Plant-Sourced Drug and Sichuan Research Center for Drug Precision Industrial Technology, West China School of Pharmacy, Sichuan University, Chengdu 610041, China

Received 15 October 2021; received in revised form 9 November 2021; accepted 20 November 2021

*Corresponding author. Tel./fax: +86 28 85502307.

E-mail address: sunxun@scu.edu.cn (Xun Sun).

Supporting Tables

Table S1 The roughness of PNs-S, PSNs-S and PSNs-R.

Sample	Ra (nm)	Rq (nm)
PNs-S	5.988	7.116
PSNs-S	5.818	6.727
PSNs-R	14.880	17.600

Ra: average roughness.
Rq: root mean square roughness.

Supporting Figures

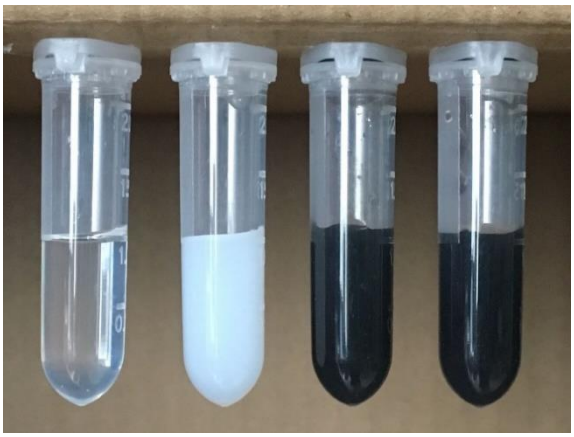

Figure S1 The appearance of synthesized nanoparticles. From left to right are PBS, SNs-R, PSNs-R and JQ-1@PSNs-R.

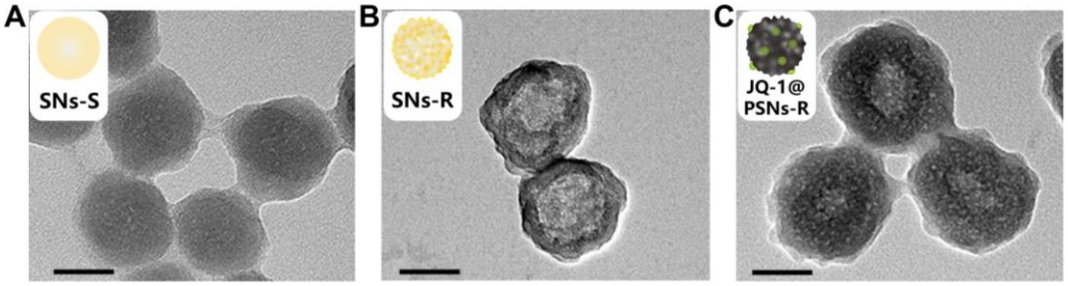

Figure S2 TEM images of (A) SNs-S, (B) SNs-R, and (C) JQ-1@PSNs-R. Transmission electron microscopy (Tecnai G2 F20 S-TWIN, FEI, Hillsboro, OH, USA) was used to characterize the morphology and structure of the nanoparticles. Scale bar = 100 nm.

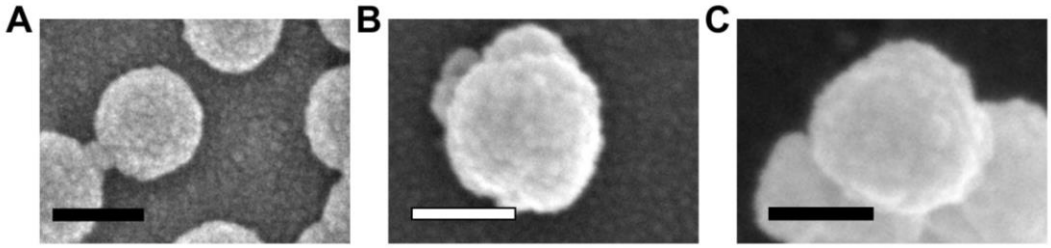

Figure S3 SEM images of (A) PNs-S, (B) PSN-S, and (C) PSN-R. A scanning electron microscope (Apreo S, Thermo Fisher Scientific, Waltham, MA, USA) was used to observe the surface of nanoparticles. Scale bar = 100 nm.

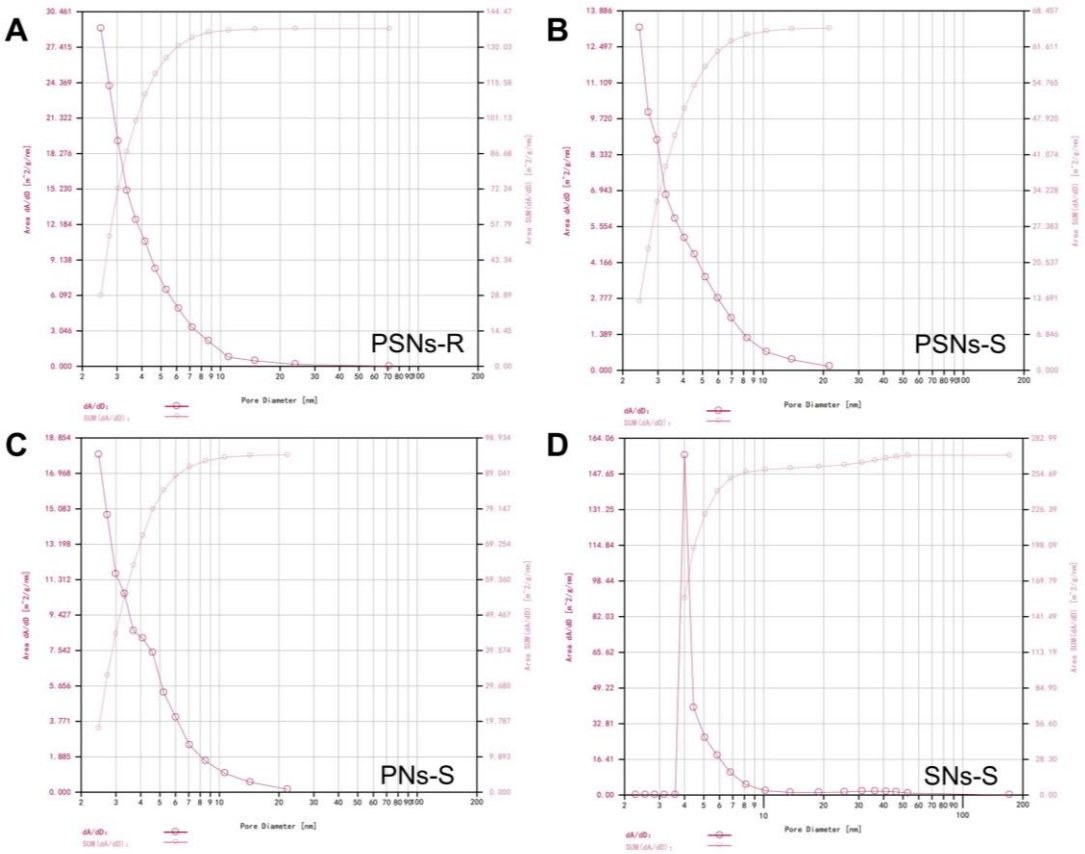

Figure S4 Mesopores of (A) PSNs-R, (B) PSNs-S, (C) PNs-S, and (D) SNs-R. The mesopore size of SNs-R was measured as 4.01 nm by nitrogen adsorption-desorption tests. PSNs-R, PSNs-S and PNs-S showed no mesopore on the surface.

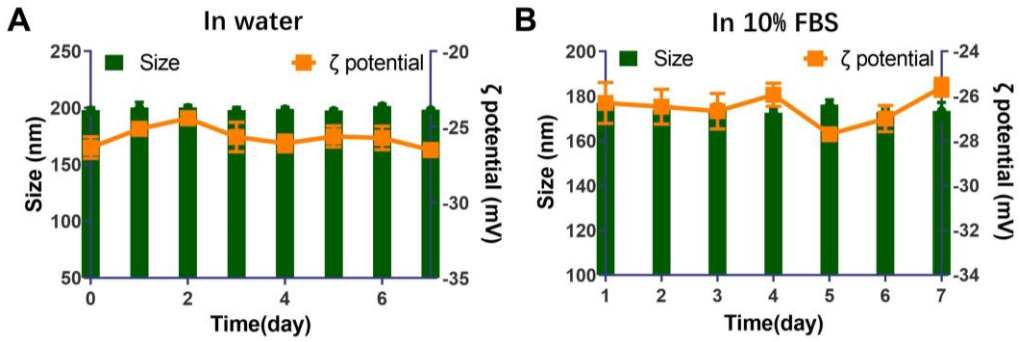

Figure S5 Stability of JQ-1@PSNs-R. JQ-1@PSNs-R were dispersed (A) in water or (B) in 10% FBS for one week. The size and ζ potential of JQ-1@PSNs-R were measured by dynamic light scattering (Zetasizer ZEN3690, Malvern, UK). Results showed that the JQ-1@PSNs-R exhibited a good stability. Data were mean ± SEM, *n* = 3.

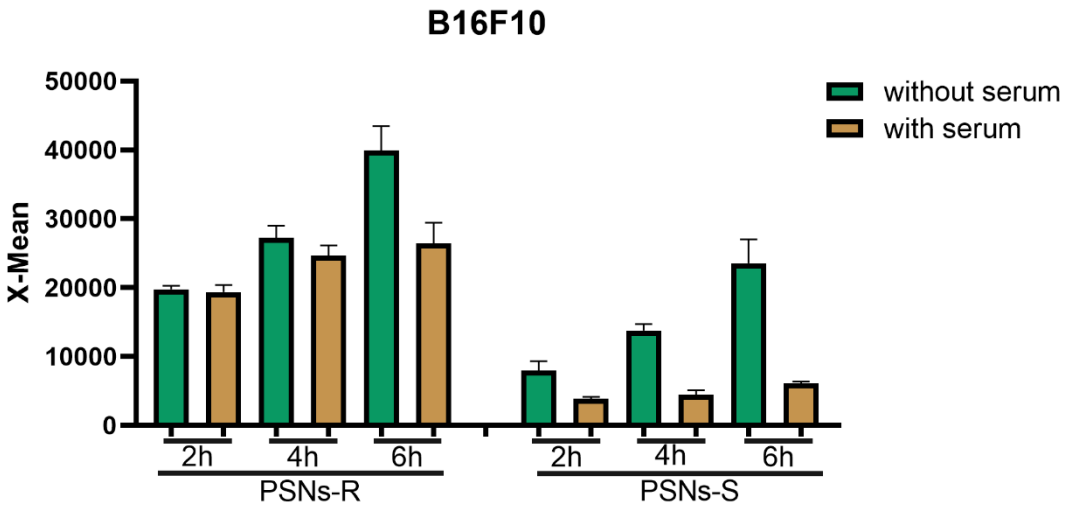

Figure S6 The uptake of PSNs-R and PSNs-S on B16F10 cells in the medium with or without serum of different uptake time. In the presence of serum, the uptake of PSNs-R and PSNs-S were both decreased. Data were mean ± SEM, $n = 3$.

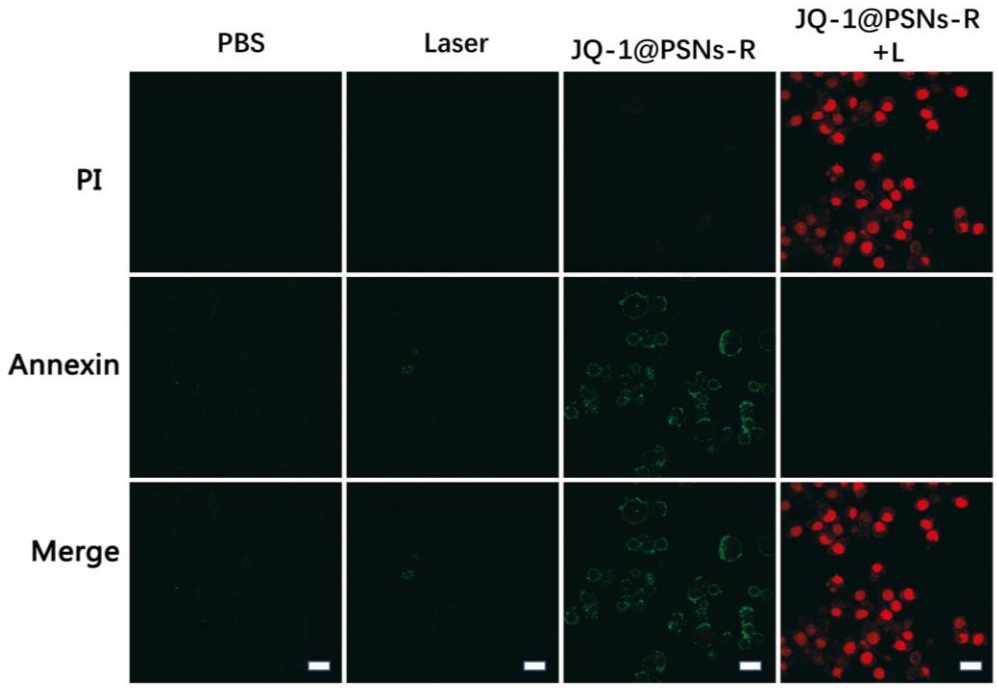

Figure S7 Photothermal cytotoxicity of JQ-1@PSNs-R. B16F10 cells were incubated in 35 mm confocal dishes for 24 h. After incubation, cells were exposed to JQ-1@PSNs-R for 1 h and irradiated for 5 min with a near-infrared laser (808 nm, 1.18 W/cm^2). After co-stained by annexin and propidium iodide, the cells were imaged by confocal laser scanning microscopy (Zeiss, Oberkochen, Germany). Scale bar = 10 μm

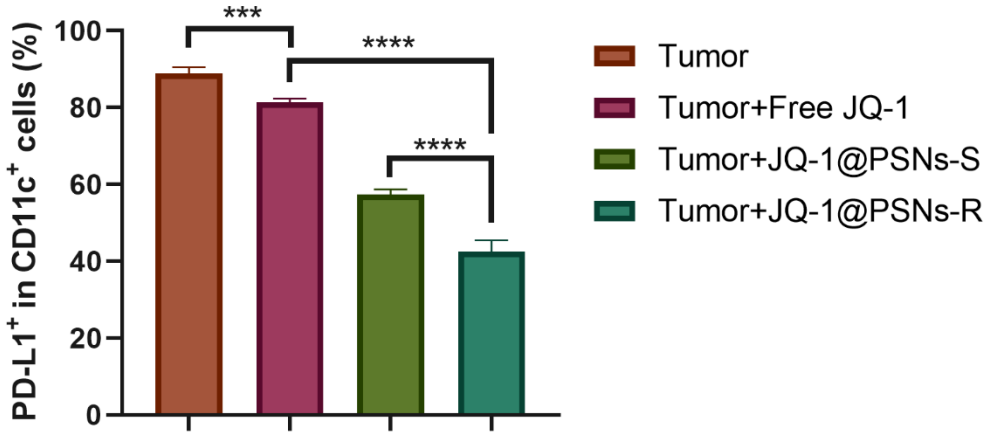

Figure S8 JQ-1@PSNs-R inhibiting the expression of PD-L1 in BMDCs. After incubated with BMDCs and tumor-related stimulants, the JQ-1@PSNs-R significantly inhibit PD-L1 expression in BMDCs which was much better than that of JQ-1@PSNs-S and free JQ-1. Data were mean ± SEM, n = 4 and analyzed by one-way ANOVA, ***P < 0.001 and ****P < 0.0001.

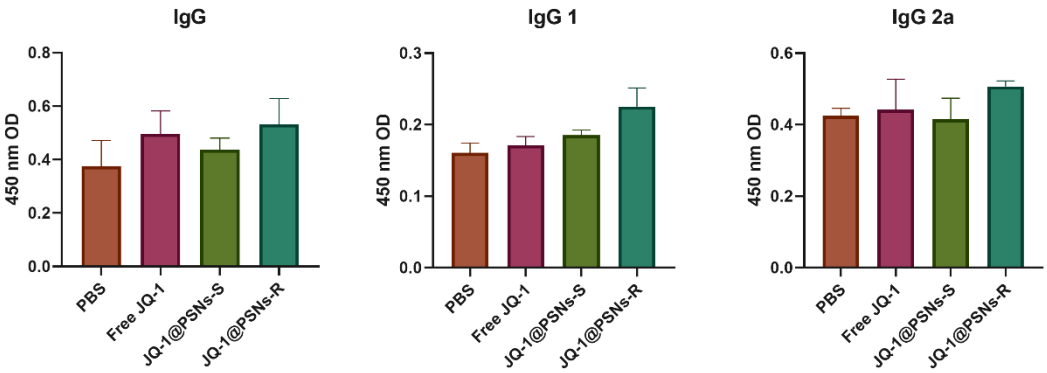

Figure S9 The antibodies in serum after JQ-1@PSNs-mediated photothermal therapy. Free JQ-1, JQ-1@PSNs-S or JQ-1@PSNs-R were intratumorally injected to mice, and at 3 days after photothermal therapy, mice serum was collected and the antibodies were detected by ELISA kits. Data were mean ± SEM, n = 3.

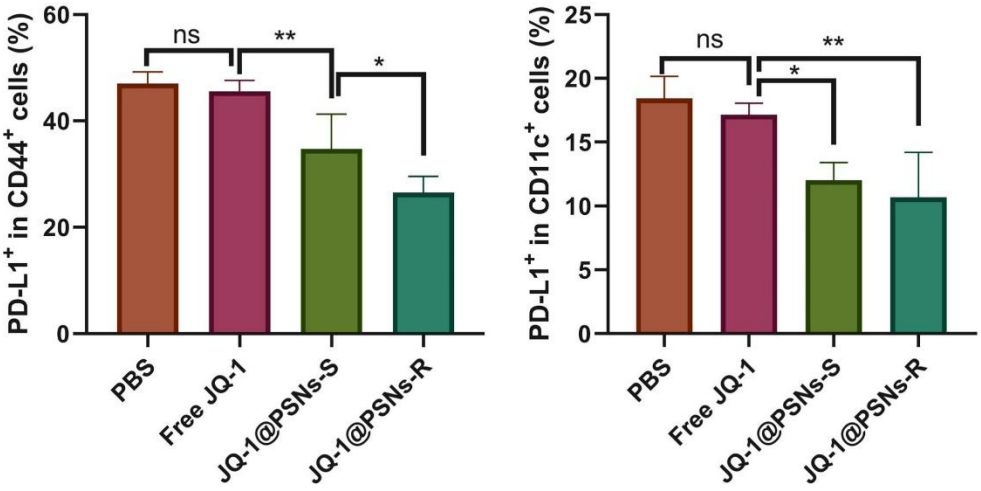

Figure S10 The expression of PD-L1 in tumor cells and DCs after JQ-1@PSNs-mediated photothermal therapy. Free JQ-1, JQ-1@PSNs-S or JQ-1@PSNs-R were intratumorally injected to mice, and at 3 days after photothermal therapy, tumor tissues were collected and the PD-L1-expressing tumor cells ($CD44^+$) and DCs ($CD11c^+$) were detected by flow cytometry. Results showed that JQ-1@PSNs-R had a better PD-L1 inhibiting effect than JQ-1@PSNs-S in tumor cells. Data were mean ± SEM, $n = 4$ and analyzed by One-way ANOVA, $^*P < 0.05$, $^{**}P < 0.01$. ns, not significant.

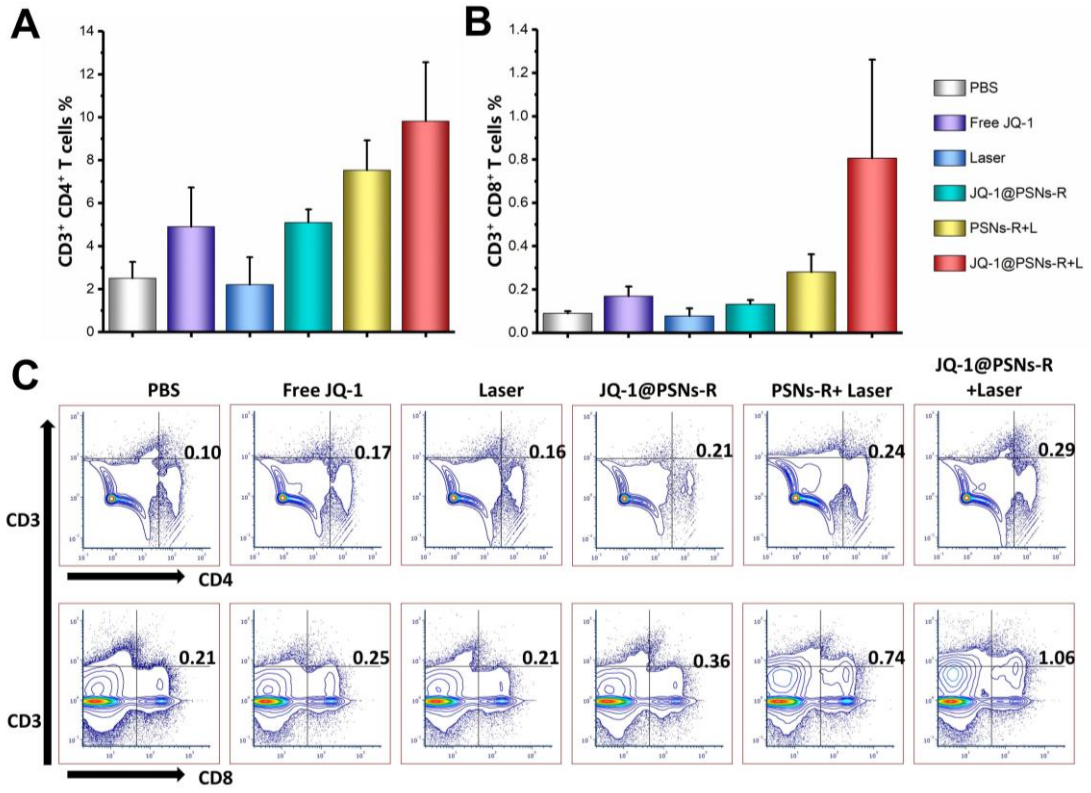

Figure S11 The proportions of CD4 and CD8 T cells in tumor sites after JQ-1@PSNs-mediated photothermal therapy. At 7 days after photothermal therapy, mice were sacrificed, and the tumor tissues were harvested. The percentage of CD4 T cells and CD8 T cells in tumor sites was measured by flow cytometry. Data were mean ± SEM, $n = 4$.

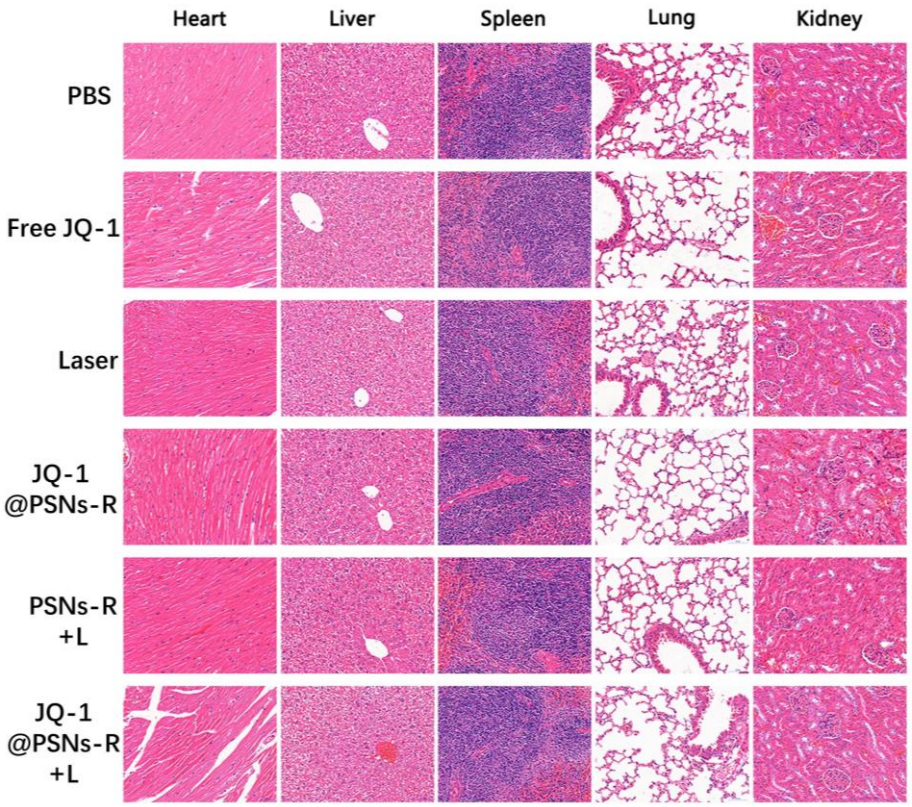

Figure S12 Histopathology examination after JQ-1@PSNs-mediated photothermal therapy. After therapy, mice were sacrificed on Day 14. Hearts, lungs, livers, spleens and kidneys were collected and stained with hematoxylin and eosin for histological analysis (HE stain, × 400).

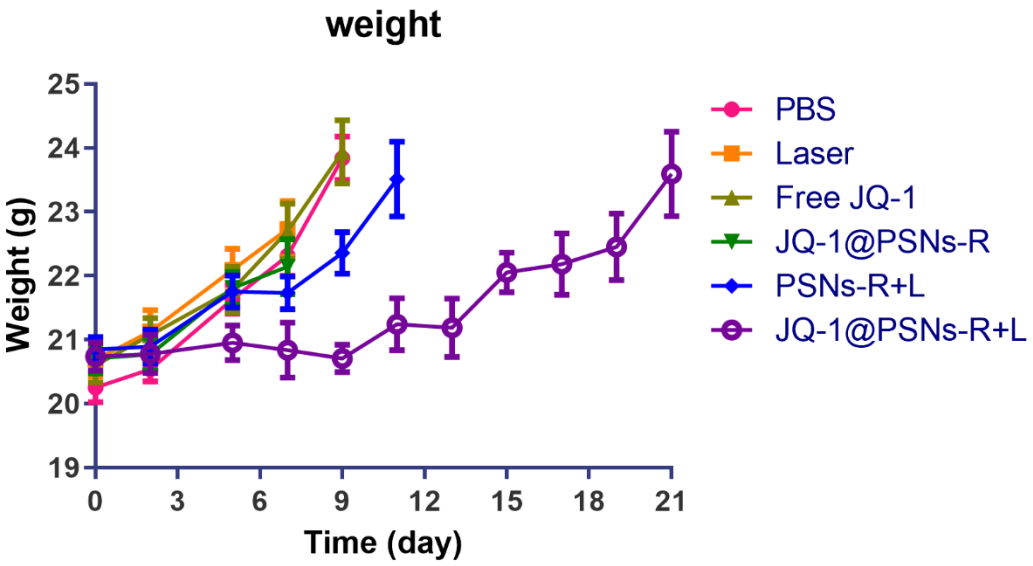

Figure S13 Mice weight after JQ-1@PSNs-mediated photothermal therapy. For weight, the data were recorded every two days until the first mouse in the group died. Data were mean ± SEM, n = 8.

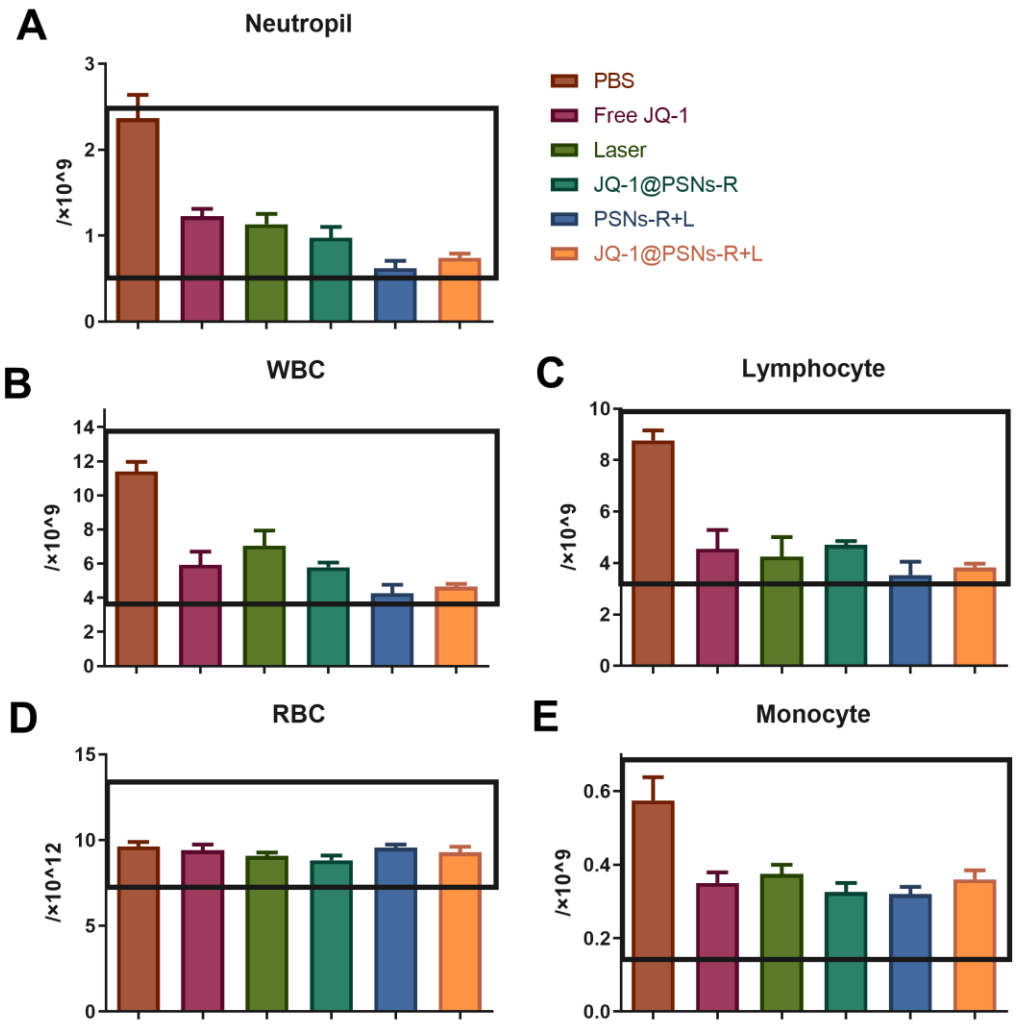

Figure S14 Analysis of cells in the blood after JQ-1@PSNs-mediated photothermal therapy. Results showed that the cells in blood were within the normal range. Data were mean ± SEM, $n = 4$.

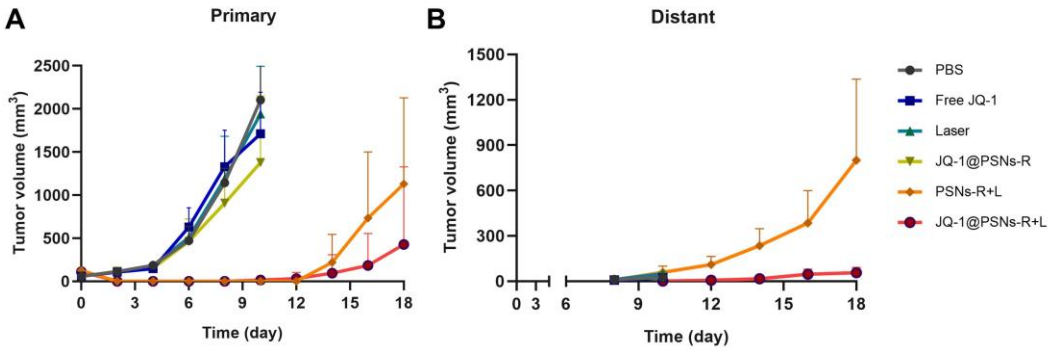

Figure S15 Inhibition of primary and distant melanoma growth in a model of distant tumor metastasis. Results showed that the bilateral tumor growth of mice in group JQ-1@PSNs-R+L was the slowest, indicating this photothermal immunotherapy led to an effective antitumor immune response. Data were mean ± SEM, $n = 5$.